GARNER, LARRY W. Study of $Y_1^*(1385)$ Decay Modes. (1974)
Directed by: Dr. G. W. Meisner and Dr. R. B. Muir. Pp. 42

The purpose of this study was to investigate the processes for the three body productions:

$$a.\ K^- p \rightarrow \Lambda\pi^+\pi^-$$

$$b.\ K^- p \rightarrow \Sigma^\circ\pi^+\pi^-$$

near the 1.670 GeV center of mass energy region. The processes studied included the quasi two body mode, i.e. $K^- p \rightarrow Y_1^*\pi$, pure phase space production and combinations of the two processes.

The $K^- p \rightarrow \Lambda\pi^+\pi^-$ reaction was determined to proceed almost entirely by the intermediate $Y_1^*\ \pi$ state. However, only 62.5% of the $K^- p \rightarrow \Sigma^\circ\pi^+\pi^-$ events were found to proceed via the Y_1^* state with the remaining events being attributed to the non-resonant phase space mode. The $Y_1^*(1385)$ branching ratio,

$$\frac{\Gamma(Y_1^* \rightarrow \Sigma^\circ\pi)}{\Gamma(Y_1^* \rightarrow \Sigma^\circ\pi) + \Gamma(Y_1^* \rightarrow \Lambda\pi)}$$

was also determined. Its value is 0.18 ± 0.02.

4

STUDY OF $Y_1^*(1385)$ DECAY MODES

by

Larry W. Garner

A Thesis Submitted to
the Faculty of the Graduate School at
The University of North Carolina at Greensboro
in Partial Fulfillment
of the Requirements for the Degree
Master of Science

Greensboro
1974

Approved by

Gerald W. Meisner
Thesis Adviser

Robert B. Mann
Thesis Adviser

APPROVAL PAGE

This thesis has been approved by the following committee of the Faculty of the Graduate School at The University of North Carolina at Greensboro.

Thesis Advisers Gerald W. Meisner

Robert B. Muir

Oral Examination Committee Member Kenneth A. Byrd

4 April '74
Date of Examination

ACKNOWLEDGMENTS

The author would like to thank Duke University for providing the data for this study. He would also like to extend his grateful appreciation to the physics department and academic computer center of the University of North Carolina for use of their facilities and for their funding. In addition, he would like to acknowledge the North Carolina Board of Science and Technology for additional funds, without which this study could not have been completed. The author would especially like to thank Dr. G. W. Meisner and Dr. R. B. Muir for their patient guidance and assistance throughout the course of his work. Finally, the author would like to thank his wife, Frances, for helping in the preparation of this manuscript.

TABLE OF CONTENTS

	Page
INTRODUCTION	1
BACKGROUND	2
PRESENCE OF RESONANCE	8
DATA ANALYSIS	17
A. Intermediate Y_1^* State in $K^- p \rightarrow \Lambda\pi^+\pi^-$	19
B. Intermediate Y_1^* State in $K^- p \rightarrow \Sigma^\circ\pi^+\pi^-$	30
SUMMARY AND CONCLUSIONS	39
FOOTNOTES AND BIBLIOGRAPHY	41
Appendix A	42

LIST OF TABLES

		Page
Table I:	Results of Best Y_1^* Fit to $K^-p \rightarrow \Lambda\pi^+\pi^-$ Events	29
Table II:	Results of Best Y_1^* Fit to $K^-p \rightarrow \Sigma^\circ\pi^+\pi^-$ Events	35
Table III:	Comparison of Experimental and World Average Values .	40

LIST OF FIGURES

Page

Figure 1: Baryon super-multiplet 6

Figure 2: Meson super-multiplet 6

Figure 3: Resonant baryon super-multiplet containing $Y_1^*(1385)$ . . 7

Figure 4: Phase space distribution function 9

Figure 5: Breit-Wigner distribution function 12

Figure 6: Dalitz Plot representing non-resonant mode 15

Figure 7: Dalitz Plot representing resonant mode 16

Figure 8: Two prong plus vee geometry 18

Figure 9: Dalitz Plot of $M^2(\Lambda,\pi^+)$ versus $M^2(\Lambda,\pi^-)$ 20

Figure 10: Pure Breit-Wigner fit to $M^2(\Lambda,\pi^+)$ histogram. Each Λ combined with π^+ 21

Figure 11: Pure Breit-Wigner fit to $M^2(\Lambda,\pi^-)$ histogram. Each Λ combined with π^- 22

Figure 12: Allocation fit to $M^2(\Lambda,\pi^+)$ histogram 25

Figure 13: Allocation fit to $M^2(\Lambda,\pi^-)$ histogram 26

Figure 14: Procedural steps for allocation fitting 28

Figure 15: Pure phase space fit to $M^2(\Sigma^\circ,\pi^+)$ histogram. Each Σ° combined with π^+ 32

Figure 16: Pure phase space fit to $M^2(\Sigma^\circ,\pi^-)$ histogram. Each Σ° combined with π^- 33

Figure 17: Dalitz Plot of $M^2(\Sigma^\circ,\pi^+)$ versus $M^2(\Sigma^\circ,\pi^-)$ 34

Figure 18: Allocation fit to $M^2(\Sigma^\circ,\pi^+)$ histogram 36

Figure 19: Allocation fit to $M^2(\Sigma^\circ,\pi^-)$ histogram 37

CHAPTER I

INTRODUCTION

During the past decades much interest has been devoted to the study of resonance production in K^-N interactions. Of particular interest are the three known resonances and four other possible resonances in the 1.600 GeV to 1.700 GeV center of mass energy region. In the former group is the $Y_1^*(1385)$ resonance. The purpose of the study described here is to determine whether or not $Y_1^*(1385)$ resonance production occurs in the $K^-p \rightarrow \Sigma^\circ\pi^+\pi^-$ reaction and if possible, to determine the $Y_1^*(1385)$ branching ratio,

$$\frac{\Gamma(Y_1^* \rightarrow \Sigma^\circ\pi)}{\Gamma(Y_1^* \rightarrow \Sigma^\circ\pi) + \Gamma(Y_1^* \rightarrow \Lambda\pi)} .$$

Data for this study originated at the Brookhaven National Laboratory Alternating Gradient Synchrotron in the form of 500,000 photographic exposures of the Columbia-BNL thirty inch liquid hydrogen bubble chamber. The bubble chamber was exposed to a K^- beam whose momentum in the center of the chamber was 0.737 GeV/c. The pictures were taken to Duke University where they were scanned and measured. The results were transferred to magnetic tapes. Other output magnetic tapes resulting from geometric and kinematic computer analysis of the raw data contain the data included in this study.

CHAPTER II

BACKGROUND

As far back as ancient Greece mankind has been striving to find some natural order in the cosmos. One facet of this drive was an attempt to determine the elementary constitutents of all the various substances that man observes. However, it was not until the 18^{th} and 19^{th} centuries that any significant breakthroughs occurred. It was in those two centuries that scientists first learned that all chemical substances could be formed from 92 naturally occurring building blocks, known as elements. Perhaps even more significant was the discovery that these elements could be grouped together into a smaller number of families, based on similar chemical properties. Thus, it began to seem as if scientists were finally accomplishing the quest of the ancient scholars. This belief was further reinforced in the late 19^{th} and early 20^{th} centuries when scientists correctly suspected that elements could be formed by combining three even more elementary particles, the newly discovered electron and proton and an undiscovered particle named the neutron. As prophesied, the neutron was isolated in 1932 by James Chadwick. However, as this picture of matter's structure was being completed, new problems were beginning to arise for the physicist.

Based on quantum mechanics, new theories were predicting the existence of a particle identical to the electron in all properties with one exception, charge. That is, the electron has a negative charge, while the new "anti-particle" has a positive charge associated with it.

In the very same year as the neutron discovery, the existence of the positron, the anti-particle of the electron, was confirmed. In the succeeding years, up to about 1960, several new particles along with their anti-particles were discovered. Some had been predicted by theories while others had not. Included in the latter were the so called "strange particles." Their strangeness arose because they lived a million million times longer than physicists had anticipated. To help account for their unexpected lifetime, scientists had to acknowledge the existence of a previously unknown force. Up to that time, there were only three recognized universal forces: the gravitational force which was described by Newton, the electromagnetic force which was summarized by Maxwell's equations, and the strong nuclear force that holds the nuclei of atoms together. Now another force called the weak nuclear force was required to explain the slow decay of the strange particles. It was reasoned that strange particles are produced only in pairs by the strong nuclear force and once the pair is separated, only the weak force can cause an individual strange particle to decay. Because it was noted that one of the decay products was always one of the group of particles called leptons, the weak force was defined as that force through which leptons interact with baryons, mesons or other leptons.

The above groupings of particles was one of physicists first attempts to find fundamental families for the elementary particles. The groupings were based primarily on the masses of the particles and to some extent on how they interact with each other. However, these three divisions and other such schemes shed little light on any underlying natural laws. Furthermore, after 1960 the groupings became even more

inadequate. For during the preceding decades, the number of particles mushroomed with the discovery of resonances.

A resonance can occur when two particles are produced with the necessary energies in a nuclear interaction. Right after production, while the particles are in close proximity, the two particles might briefly stick together to form a resonance. For the sake of a mental picture, this process can be thought of in the following manner. As one particle is passing close to another, it is captured and the two oscillate (thus, the term resonance) around each other. After a very short time, the two particles break apart and go their separate ways.

With the discovery of resonances, it became necessary not only to look for natural groupings of stable particles and their anti-particles, but also to devise a scheme that would include the resonances. Today the search has not yet been completed. However, two major advances have been made toward that goal.

The first was the realization that some of the previously accepted particles were in fact nothing more than different states of the same particle called a multiplet. For example the proton and neutron are just different charged states of a kind of multiplet known as a doublet. The pions, π^+, π^- and π° are the possible charged states of a type of multiplet known as a triplet. The realization followed logically from the fact that charge plays no part in nuclear interactions. All nuclear reactions are dominated entirely by either the weak or strong nuclear force. The only effect electric charge has on nuclear interactions is that it absolutely forbids any reactions which would not conserve electric charge.

The other advancement was the development of SU(3) theory which organizes particles into families called super-multiplets. Diagrams of the baryon and meson super-multiplets are given in Figures 1 and 2 respectively. A quantum number (isotopic spin) which is related to electric charge is plotted along the horizontal axis. The parameter plotted vertically is hypercharge, twice the average charge of each multiplet. Figure 3 shows the baryon resonance super-multiplet that contains the $Y_1^*(1385)$, about which this study is concerned.

SU(3) is an elaborate mathematical treatment of group theory which is used to explain the number of observed particles in the super-multiplets. It was derived independently by Murray Gell-Mann and Yuval Ne'eman in 1961. One of the main advantages of SU(3) is that the mathematical treatment devised by them not only explains the number, but also predicts the masses and decay modes of the unstable particles in a super-multiplet. Unfortunately, SU(3) leaves unanswered many questions about the nature and significance of the super-multiplets. Nevertheless, SU(3) has been a major step toward finding some natural order in the seeming choas of elementary particles.

Figure 1: Baryon super-multiplet.

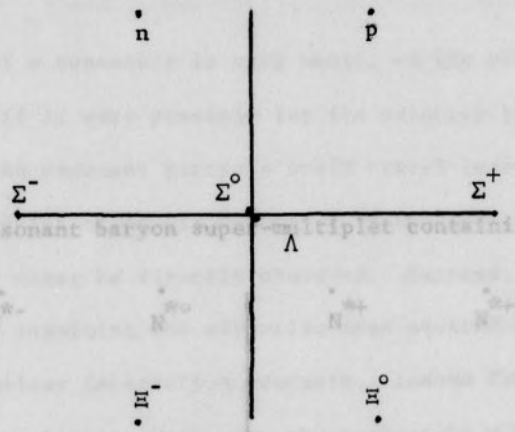

Figure 2: Meson super-multiplet.

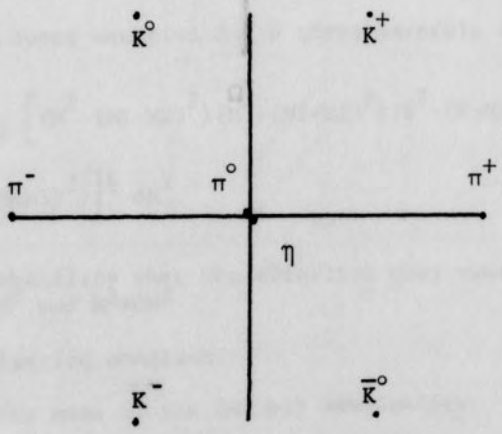

Figure 3: Resonant baryon super-multiplet containing $Y_1^*(1385)$.

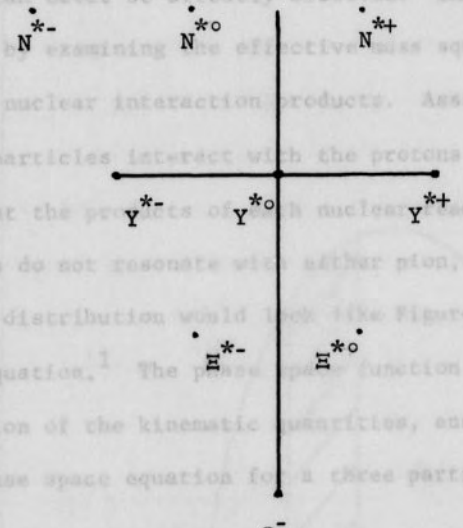

CHAPTER III

PRESENCE OF RESONANCE

The lifetime of a resonance is very small, on the order of 10^{-23} seconds. Thus, even if it were possible for its velocity to be that of the speed of light, the resonant particle would travel less than 10^{-12} centimeters from its point of origin before it breaks apart or decays. Hence a resonance can never be directly observed. Instead, its presence is determined by examining the effective mass squared distributions of combinations of nuclear interaction products. Assume for the moment, that a beam of K^- particles interact with the protons in a hydrogen bubble chamber and that the products of each nuclear reaction were a Λ, π^+ and π^-. If the Λ's do not resonate with either pion, then the effective (Λ,π) mass squared distribution would look like Figure 4 and be described by a phase space equation.[1] The phase space function is derived solely from the conservation of the kinematic quantities, energy and momentum. The form of the phase space equation for a three particle final state is

$$PS(M^2) = \frac{N}{(E*M)^2}\left[(M^2-(M1-M2)^2)(M^2-(M1+M2)^2)(E^2-(M-M3)^2)\right.$$
$$\left.(E^2-(M+M3)^2)\right]^{\frac{1}{2}}\, dM^2$$

where $PS(M^2)$ = the probability that the effective mass squared is between M^2 and M^2+dM^2

N = normalization constant

M = effective mass of the (M1,M2) combination

E = total energy involved in the reaction

Figure 4: Phase space distribution function.

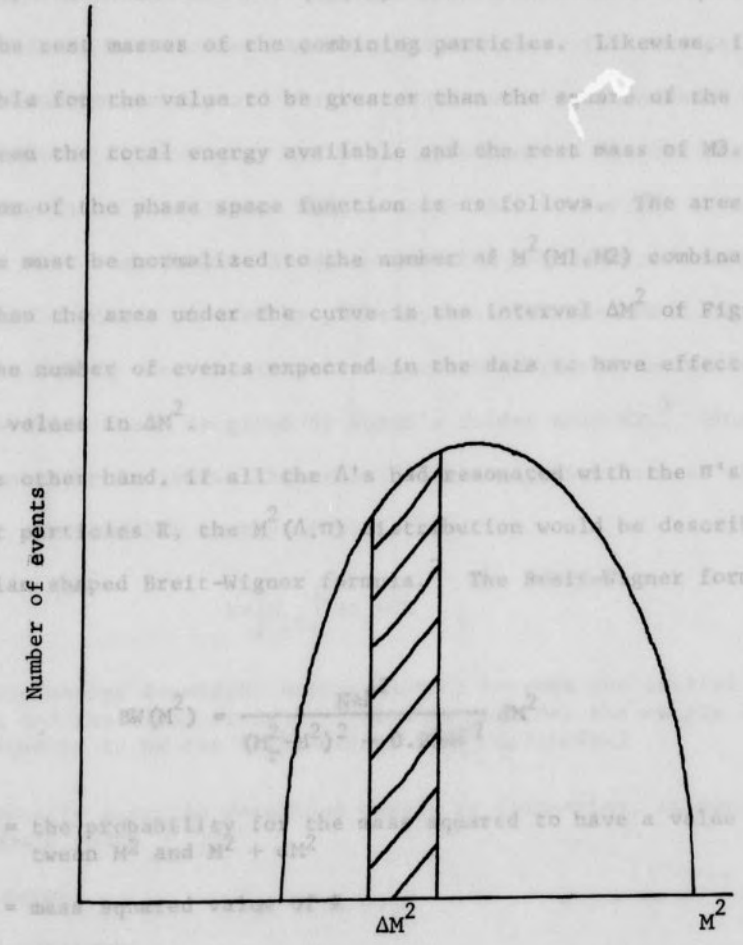

M1, M2 = masses of the two particles which are being paired

M3 = mass of third particle.

The function is bound between a lower limit of $M^2 = (M1+M2)^2$ and an upper limit of $M^2 = (E-M3)^2$. This is apparent when one considers that it is impossible to have a $M^2(M1,M2)$ value less than the square of the sum of the rest masses of the combining particles. Likewise, it is also impossible for the value to be greater than the square of the difference between the total energy available and the rest mass of M3. The interpretation of the phase space function is as follows. The area under the curve must be normalized to the number of $M^2(M1,M2)$ combinations observed. Then the area under the curve in the interval ΔM^2 of Figure 4 represents the number of events expected in the data to have effective mass squared values in ΔM^2.

On the other hand, if all the Λ's had resonated with the π's to form resonant particles R, the $M^2(\Lambda,\pi)$ distribution would be described by the Gaussian shaped Breit-Wigner formula.[2] The Breit-Wigner formula is

$$BW(M^2) = \frac{N*\Gamma^2}{(M_r^2-M^2)^2 + 0.25*\Gamma^2}\, dM^2$$

where $BW(M^2)$ = the probability for the mass squared to have a value between M^2 and $M^2 + dM^2$

M^2 = mass squared value of R

M_r^2 = central value of R

Γ = full width of the Breit-Wigner function at half maximum height

N = normalization constant.

When the area under the Breit-Wigner curve has been normalized to the number of observed R's, the area under the curve bounded by the interval ΔM^2 (see Figure 5) is the number of resonances expected with mass squared values in ΔM^2.

Thus, to determine if there are intermediate resonant states, all one has to do is to see whether the Breit-Wigner curve fits the data. If it does, then one can say all the events proceeded by a resonant state. However, if neither Breit-Wigner nor phase space curves fit the data, and since there is no requirement which states that either all or none of the events must resonate, it is quite possible that some events form a resonance while others proceed by phase space. This can best be understood by realizing that the transition probability from an initial state to some final state is given by Fermi's Golden Rule #2.[3] This quantum mechanical rule states that the transition probability is the integral over all possible energy states of

$$k * \left|M_{if}\right|^2 * \rho_E * dE$$

where M_{if} = the energy dependent matrix element between the initial state i and the final state f. (Here we consider the matrix element squared to be the Breit-Wigner (BW) amplitude.)

ρ_E = density function described purely by kinematics, in our case, phase space

E = energy

k = a constant.

If $\left|M_{if}\right|^2$ is a constant, the probability distribution is described by phase space. On the other hand, if ρ_E is a constant over the energy interval, then the probability distribution is proportional to $\left|M_{if}\right|^2$ which is equal to $BW(M^2)$. However, if neither term is a constant, then

Figure 5: Breit-Wigner distribution function.

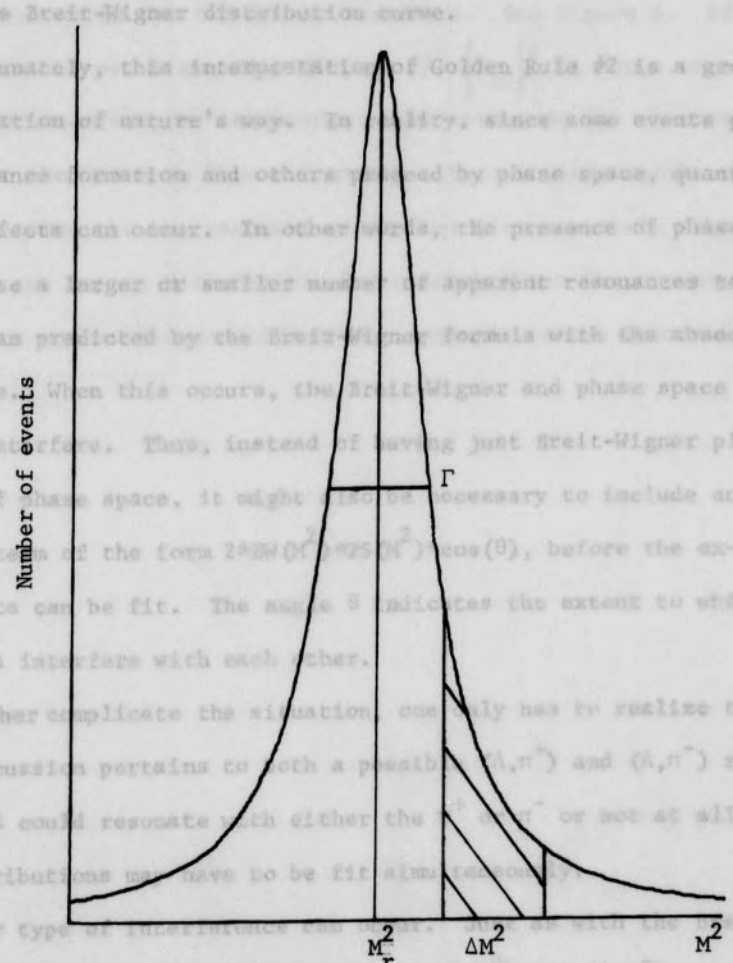

the distribution must be described by some combination of phase space and Breit-Wigner. The simplest possible combination would be to add Breit-Wigner and phase space curves in some proportion to fit the experimental data. The number of resonant states would then be the area under just the Breit-Wigner distribution curve.

Unfortunately, this interpretation of Golden Rule #2 is a gross oversimplification of nature's way. In reality, since some events proceed by resonance formation and others proceed by phase space, quantum mechanical effects can occur. In other words, the presence of phase space can cause a larger or smaller number of apparent resonances to be created than predicted by the Breit-Wigner formula with the absence of phase space. When this occurs, the Breit-Wigner and phase space are said to interfere. Thus, instead of having just Breit-Wigner plus some amount of phase space, it might also be necessary to include an interference term of the form $2*BW(M^2)*PS(M^2)*\cos(\theta)$, before the experimental data can be fit. The angle θ indicates the extent to which the amplitudes interfere with each other.

To further complicate the situation, one only has to realize that the above discussion pertains to both a possible (Λ,π^+) and (Λ,π^-) resonance. The Λ could resonate with either the π^+ or π^- or not at all. Thus two distributions may have to be fit simultaneously.

Another type of interference can occur. Just as with the Breit-Wigner and phase space, if the two resonances (Λ,π^+) and (Λ,π^-), are both produced in the same mass squared region, then interference can occur between the Breit-Wigner functions which describe the two resonant states. If none of the above models fit the experimental data, then interferences between the two resonances should be considered.

An examination of the $M^2(\Lambda,\pi^+)$ versus $M^2(\Lambda,\pi^-)$ graph, known as the Dalitz Plot,[4] will give some indication of whether or not any interference has occurred. If $\left|M_{if}\right|^2$ is a constant, the points on the Dalitz Plot will be uniformly distributed; that is, pure phase space leads to a uniform distribution in the two energy variables. See Figure 6. If the density of points is not a constant (Figure 7), $\left|M_{if}\right|^2$ is not a constant with energy and therefore one can suspect that resonance has occurred. Furthermore, if the bands in Figure 7 overlap, then it is possible that interference between the two resonant states has also occurred. Thus, an examination of the Dalitz Plot reveals information about the presence of a resonant state and some indication of the dynamics of the interaction.

Figure 6: Dalitz Plot representing non-resonant mode.

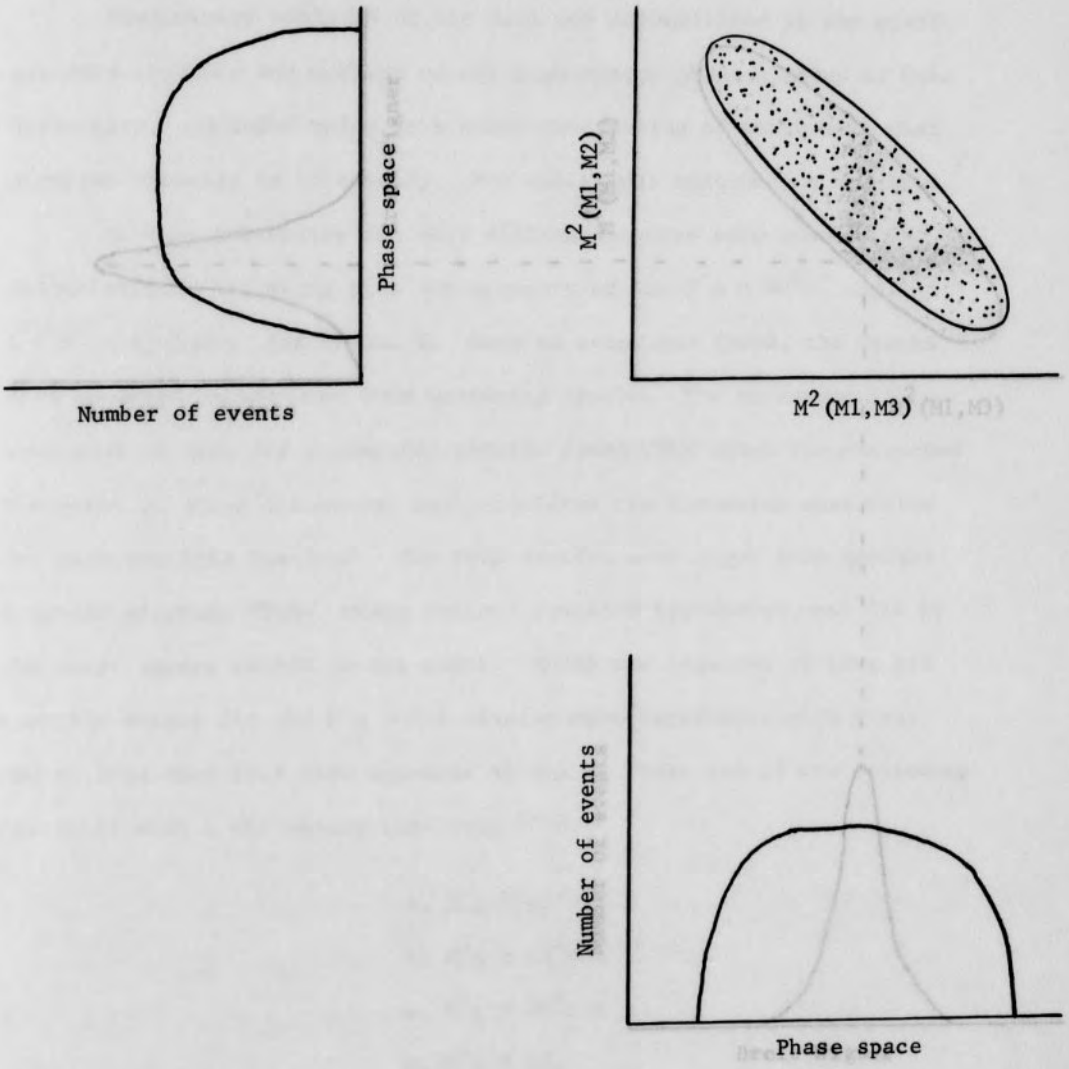

Figure 7: Dalitz Plot representing resonant mode.

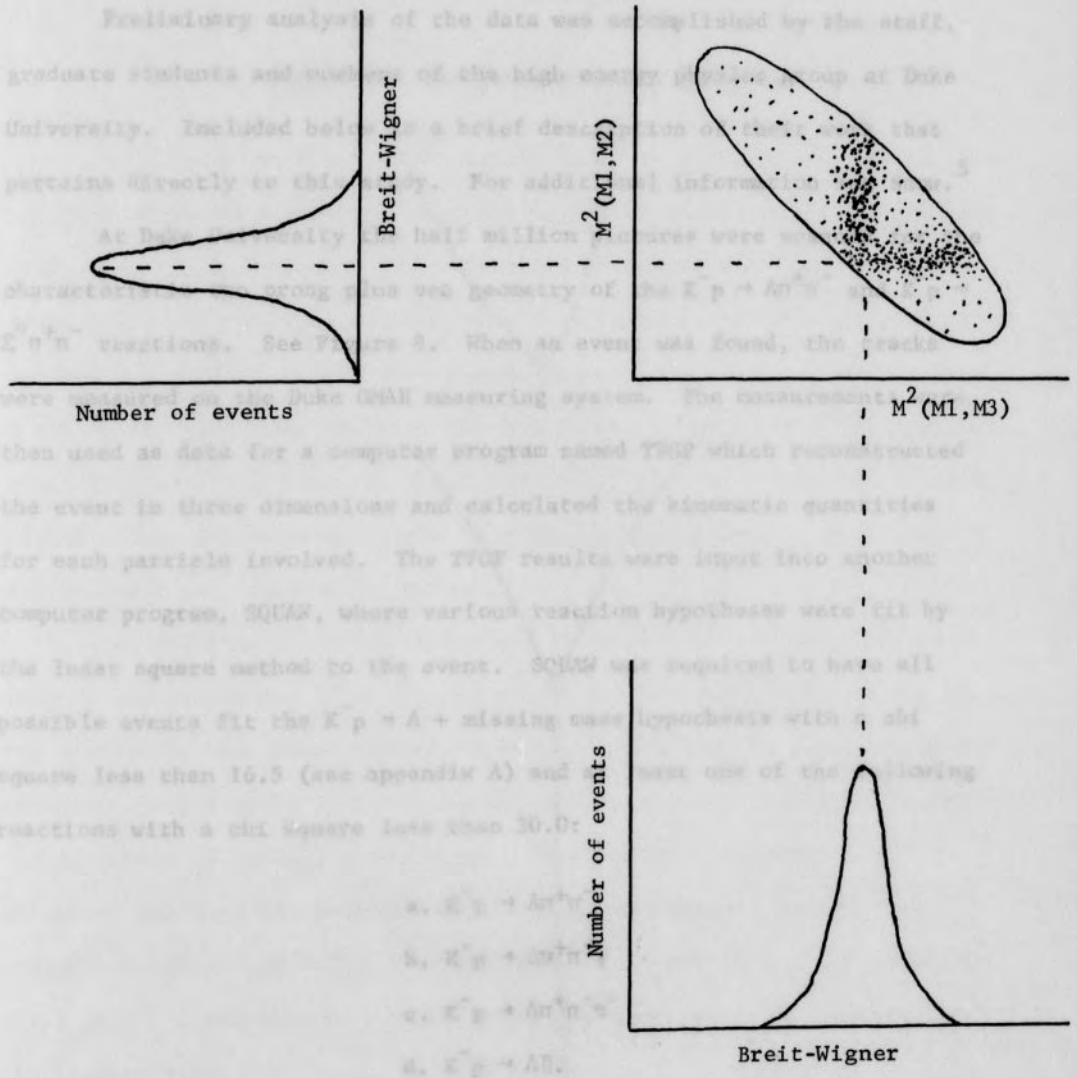

CHAPTER IV

DATA ANALYSIS

Preliminary analysis of the data was accomplished by the staff, graduate students and workers of the high energy physics group at Duke University. Included below is a brief description of their work that pertains directly to this study. For additional information see Snow.[5]

At Duke University the half million pictures were scanned for the characteristic two prong plus vee geometry of the $K^-p \rightarrow \Lambda\pi^+\pi^-$ and $K^-p \rightarrow \Sigma^\circ\pi^+\pi^-$ reactions. See Figure 8. When an event was found, the tracks were measured on the Duke OMAR measuring system. The measurements were then used as data for a computer program named TVGP which reconstructed the event in three dimensions and calculated the kinematic quantities for each particle involved. The TVGP results were input into another computer program, SQUAW, where various reaction hypotheses were fit by the least square method to the event. SQUAW was required to have all possible events fit the $K^-p \rightarrow \Lambda$ + missing mass hypothesis with a chi square less than 16.5 (see appendix A) and at least one of the following reactions with a chi square less than 30.0:

a. $K^-p \rightarrow \Lambda\pi^+\pi^-$

b. $K^-p \rightarrow \Lambda\pi^+\pi^-\gamma$

c. $K^-p \rightarrow \Lambda\pi^+\pi^-\pi^\circ$

d. $K^-p \rightarrow \Lambda\eta$.

Of the scanned events, 15,677 events met this requirement. Along with this restriction, the events were also required to have their production

Figure 8: Two prong plus vee geometry.

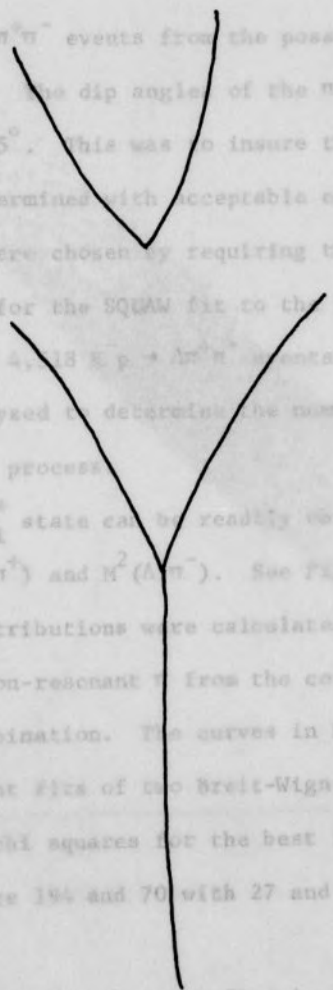

and decay vertices in a certain fiducial volume so that the beam and decay tracks would be well measured. After the above cuts, there remained 12,549 possible $K^- p \rightarrow \left\{ \begin{matrix} \Sigma^\circ \\ \Lambda \end{matrix} \right\} \pi^+\pi^-$ candidates. The $\Sigma^\circ\pi^+\pi^-$ events are considered in section B. The $\Lambda\pi^+\pi^-$ candidates are discussed below.

A. Intermediate Y_1^* State in $K^- p \rightarrow \Lambda\pi^+\pi^-$

To select the $K^- p \rightarrow \Lambda\pi^+\pi^-$ events from the possible candidates, two other criteria were imposed. The dip angles of the π^+ and π^- tracks were restricted to be less than 85°. This was to insure that the momenta of the π particles could be determined with acceptable errors. Finally, the desired $K^- p \rightarrow \Lambda\pi^+\pi^-$ events were chosen by requiring that the events have a chi square less than 12.0 for the SQUAW fit to the $K^- p \rightarrow \Lambda\pi^+\pi^-$ hypothesis. This netted a total of 4,518 $K^- p \rightarrow \Lambda\pi^+\pi^-$ events. This is the sample of events which was analyzed to determine the number of events which follow the $K^- p \rightarrow Y_1^*\pi \rightarrow \Lambda\pi^+\pi^-$ process.

The presence of the Y_1^* state can be readily observed in the mass squared distributions, $M^2(\Lambda,\pi^+)$ and $M^2(\Lambda,\pi^-)$. See Figures 9, 10 and 11. The masses for the above distributions were calculated by subtracting the momentum and energy of the non-resonant π from the corresponding kinematic quantities of the $K^- p$ combination. The curves in Figures 10 and 11 represent the best independent fits of two Breit-Wigners to the mass squared distributions. The chi squares for the best fits to the $M^2(\Lambda,\pi^+)$ and $M^2(\Lambda,\pi^-)$ distributions are 194 and 70 with 27 and 28 degrees of freedom respectively.

One possible explanation for the poor fits is that coherent interference had occurred between the Breit-Wigner amplitudes and phase space.

Figure 9: Dalitz Plot of $M^2(\Lambda,\pi^+)$ versus $M^2(\Lambda,\pi^-)$.

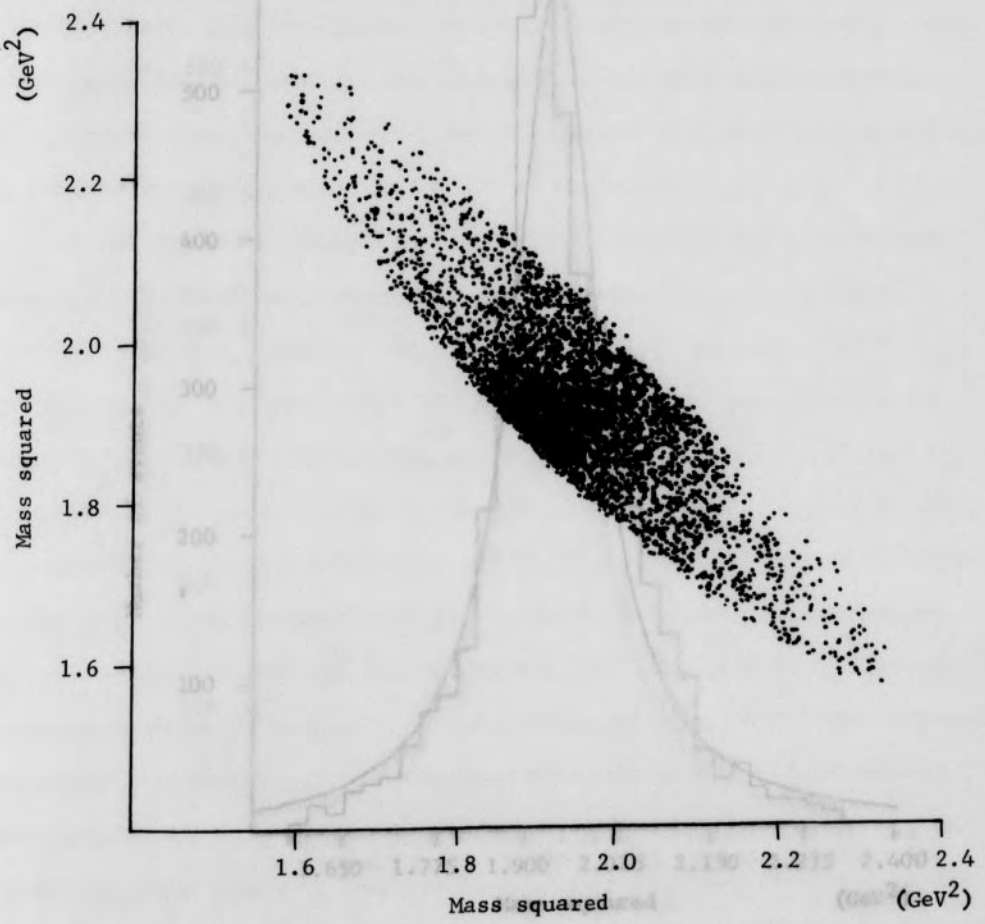

Figure 10: Pure Breit-Wigner fit to $M^2(\Lambda,\pi^+)$ histogram. Each Λ combined with π^+.

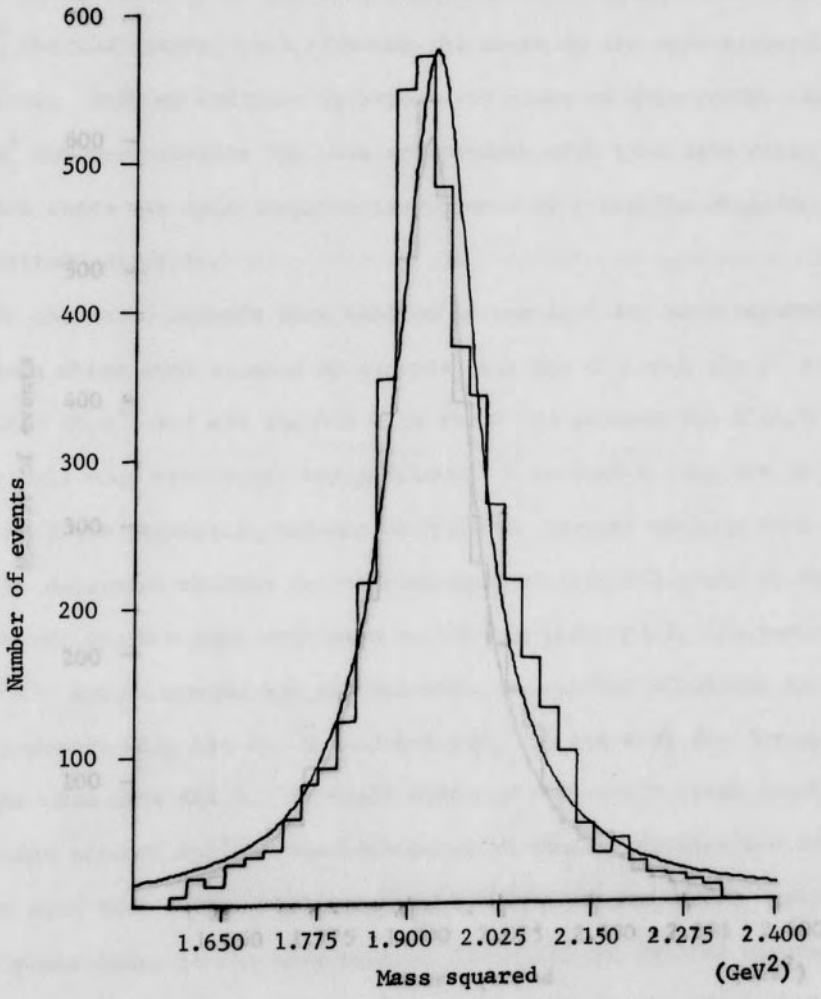

Figure 11: Pure Breit-Wigner fit to $M^2(\Lambda,\pi^-)$ histogram. Each Λ combined with π^-.

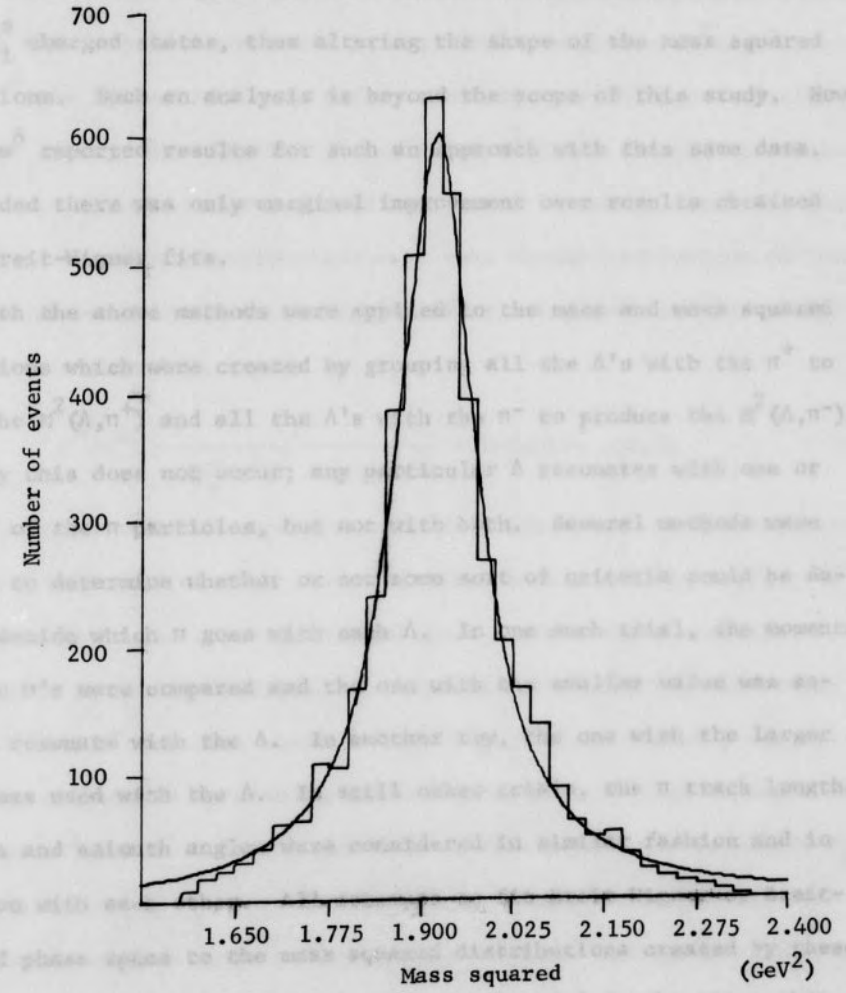

However, when an attempt was made to fit the mass squared distributions with such a hypothesis, the best fit yielded a zero coefficient for the phase space term. Hence there could be no interference with phase space.

Since the $M^2(\Lambda,\pi^+)$ and $M^2(\Lambda,\pi^-)$ distributions strongly overlap on the Dalitz Plot, it is quite possible that there was interference between the two Y_1^* charged states, thus altering the shape of the mass squared distributions. Such an analysis is beyond the scope of this study. However, Snow[6] reported results for such an approach with this same data. He concluded there was only marginal improvement over results obtained by pure Breit-Wigner fits.

Both the above methods were applied to the mass and mass squared distributions which were created by grouping all the Λ's with the π^+ to produce the $M^2(\Lambda,\pi^+)$ and all the Λ's with the π^- to produce the $M^2(\Lambda,\pi^-)$. In reality this does not occur; any particular Λ resonates with one or the other of the π particles, but not with both. Several methods were attempted to determine whether or not some sort of criteria could be deduced to decide which π goes with each Λ. In one such trial, the momenta of the two π's were compared and the one with the smaller value was assigned to resonate with the Λ. In another try, the one with the larger momentum was used with the Λ. In still other trials, the π track lengths, dip angles and azimuth angles were considered in similar fashion and in combination with each other. All attempts to fit Breit-Wigner or Breit-Wigner and phase space to the mass squared distributions created by these criteria proved unsuccessful. They were unsuccessful in the sense that the chi squares of these trials were of the same magnitude or of a much larger one than the values reported when all the Λ's were combined with each π.

Finally we were able to obtain $M^2(\Lambda,\pi^+)$ and $M^2(\Lambda,\pi^-)$ distributions that could be fit by some theoretical model with much smaller chi squares (larger confidence levels) than had previously been accomplished in this research. It was thought that the correct mass squared distributions would be obtained by allocating part of each event to form a positive, $M^2(\Lambda,\pi^+)$, histogram and the other part to form a negative, $M^2(\Lambda,\pi^-)$, histogram.[7,8] The allocations were based on the theoretical probabilities of each event having the effective $M^2(\Lambda,\pi^+)$ and $M^2(\Lambda,\pi^-)$ values. To begin the procedure, it was assumed (based on Figures 10 and 11) that the actual positive and negative distributions were some linear combination of Breit-Wigner and phase space distribution functions. The form for the positive and negative theoretical curves is

$$F^{\pm}(M^2) = \frac{\Gamma^2}{(M_r^2-M^2)^2 + 0.25*\Gamma^2} + R*(\text{phase space})$$

where R times phase space represents the relative amount of non-resonance. A sign on F indicates whether the theoretical function is to correspond to the positive or the negative distribution. After the parameters, Γ, M_r and R were chosen to determine the expressions F^+ and F^-, the probabilities P^+ and P^- for each event to have $M^2(\Lambda,\pi^+)$ and $M^2(\Lambda,\pi^-)$ respectively were calculated by placing the effective positive and negative mass squares into F^+ and F^-. The P^+ and P^- were then normalized to values P_n^+ and P_n^- such that $P_n^+ + P_n^- = 1$. It was these values P_n^+ and P_n^- which were assigned to the proper bins to form the experimental histograms. See Figures 12 and 13. For example, if the normalized probability, P_n^+, of an event having a positive mass squared of 1.92 GeV^2 is 0.73, then the height of the positive histogram bin which surrounds 1.92 GeV^2 was increased by adding 0.73. Likewise for the same event, the P_n^- of 0.27 was added to the

Figure 12: Allocation fit to $M^2(\Lambda,\pi^+)$ histogram.

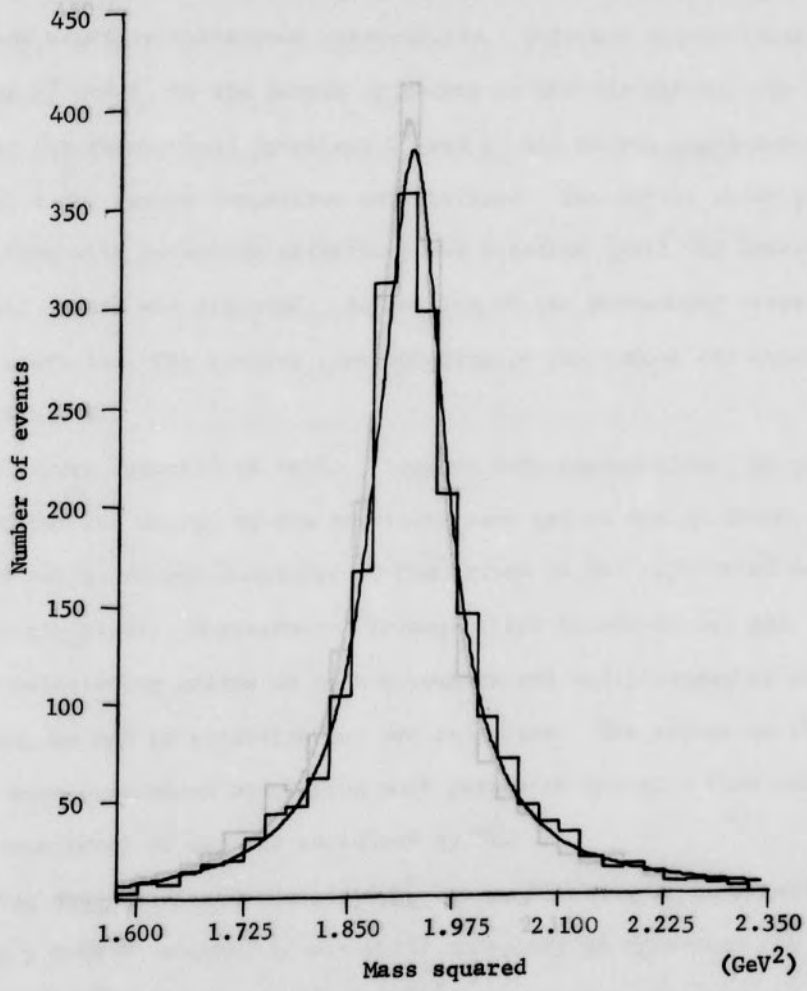

Figure 13: Allocation fit to $M^2(\Lambda,\pi^-)$ histogram.

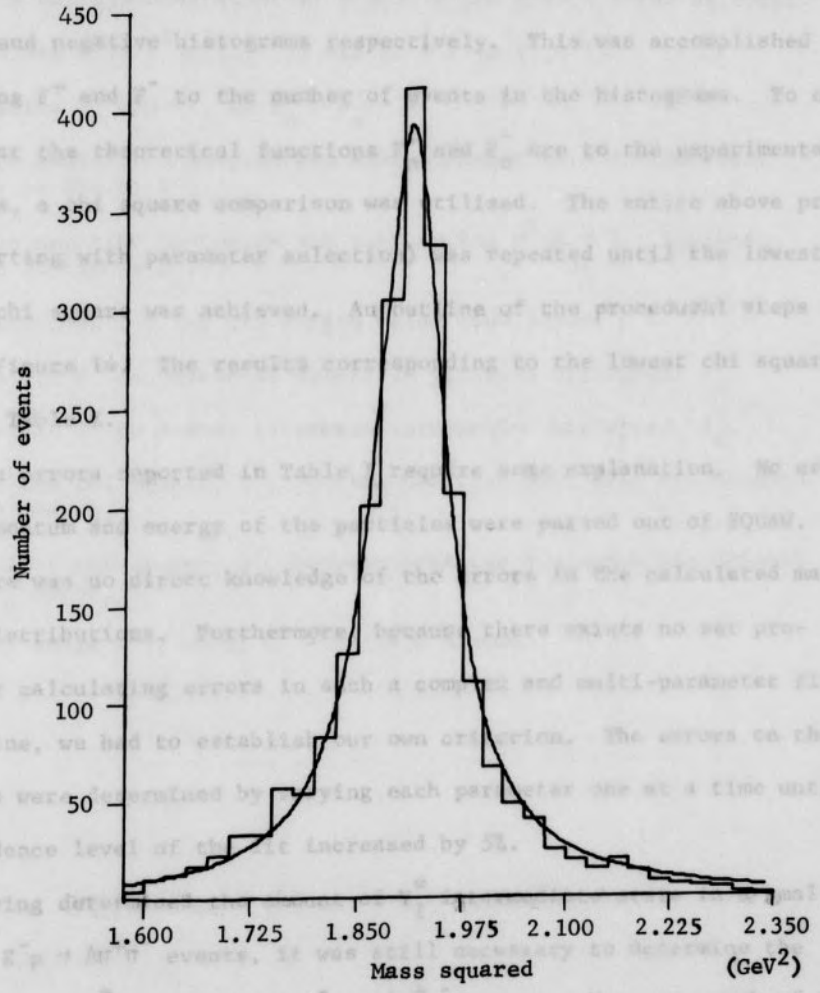

value of the appropriate negative histogram bin. The above steps were repeated until all events were considered and the experimental histograms were built. Before any comparison could be made between these histograms and the F^+ and F^- distribution functions, it was necessary to have the same number of events represented under the F^+ and F^- curves as in the positive and negative histograms respectively. This was accomplished by normalizing F^+ and F^- to the number of events in the histograms. To check how similar the theoretical functions F_n^+ and F_n^- are to the experimental histograms, a chi square comparison was utilized. The entire above process (starting with parameter selection) was repeated until the lowest possible chi square was achieved. An outline of the procedural steps is shown in Figure 14. The results corresponding to the lowest chi square appear in Table I.

The errors reported in Table I require some explanation. No errors in the momentum and energy of the particles were passed out of SQUAW. Hence there was no direct knowledge of the errors in the calculated mass squared distributions. Furthermore, because there exists no set procedure for calculating errors in such a complex and multi-parameter fitting routine, we had to establish our own criterion. The errors on the parameters were determined by varying each parameter one at a time until the confidence level of the fit increased by 5%.

Having determined the amount of Y_1^* intermediate state in a small sample of $K^-p \rightarrow \Lambda\pi^+\pi^-$ events, it was still necessary to determine the total number of Y_1^*'s in all the $K^-p \rightarrow \Lambda\pi^+\pi^-$ events. However, much of the information needed to calculate the appropriate weighting factor was not available to this study. Thus we were forced to utilize the same weight factors Snow had used for this data. Snow's weighting factor[9] is a prod-

Figure 14: Procedural steps for allocation fitting

1. Choose Γ^+, M_r^+, Γ^-, M_r^- and R for F^+ and F^-.
2. Obtain experimental value of $M^2(\Lambda,\pi^+)$ and $M^2(\Lambda,\pi^-)$ for an event.
3. Calculate $P^+ = F^+(M^2(\Lambda,\pi^+))$ and $P^- = F^-(M^2(\Lambda,\pi^-))$.
4. Normalize P^+ and P^-, so $P_n^+ + P_n^- = 1$.
5. Locate positive histogram bin surrounding $M^2(\Lambda,\pi^+)$. Increase value of bin by P_n^+.
6. Locate negative histogram bin surrounding $M^2(\Lambda,\pi^-)$. Increase value of bin by P_n^-.
7. Repeat steps 2-6 for all events being considered.
8. Normalize F^+ to number of events in positive histogram, F_n^+.
9. Normalize F^- to number of events in negative histogram, F_n^-.
10. Calculate chi square, C^+, between positive histogram bin heights and F_n^+ curve.
11. Calculate chi square, C^-, between negative histogram bin heights and F_n^- curve.
12. Repeat steps 1-11 until $C^+ + C^-$ is a minimum.

Table I: Results of Best Y_1^* Fit to $K^-p \rightarrow \Lambda\pi^+\pi^-$ Events

Quantity	Best Fit Value	Error
Chi Square	68	
Degrees of Freedom	55	
Confidence Level	16%	
Y_1^{*+} Mass^2	1.919	±0.010
Y_1^{*+} Width	0.100	±0.002
Y_1^{*-} Mass^2	1.911	±0.008
Y_1^{*-} Width	0.098	±0.002
Percent Phase Space	1.5%	
Number of Y_1^*	4,450	

uct of several weights and is equal to 3.37. The breakdown of the factor is as follows; 1.21 for events having the Λ decay outside the fiducial volume, 1.53 for events in which the Λ decayed into $n\pi^{\circ}$, 1.05 for events lost during scanning, 1.16 for events lost during TVGP processing, 1.16 for events ignored by the dip angle restriction and 1.29 to compensate for events lost by the selection criteria. Upon weighting each of the 4,450 Y_1^* states found in the $K^-p \rightarrow \Lambda\pi^+\pi^-$ sample by 3.37, it was found that 14,997 events had proceeded by the $K^-p \rightarrow Y_1^*\pi \rightarrow \Lambda\pi^+\pi^-$ process.

B. Intermediate Y_1^* State in $K^-p \rightarrow \Sigma^{\circ}\pi^+\pi^-$

The selection of the $K^-p \rightarrow \Sigma^{\circ}\pi^+\pi^-$ events from the possible candidates was completed by imposing three additional constraints. The π dip angles were required to be less than 85° to insure that the momenta of the π's were determined with acceptable errors. Because SQUAW was not required to fit the data to the $K^-p \rightarrow \Sigma^{\circ}\pi^+\pi^-$ hypothesis, an indirect determination for that event type had to be made. Since the Σ° decays within 10^{-15} seconds into a Λ and γ, each possible candidate was required instead to fit the SQUAW $K^-p \rightarrow \Lambda\pi^+\pi^-\gamma$ hypothesis with a chi square less than 30.0. However, this latter criterion left two remaining sources of contamination in the sample. Due to the fact that the $K^-p \rightarrow \Lambda\pi^+\pi^-$ hypothesis is much more difficult to fit in SQUAW than the $K^-p \rightarrow \Lambda\pi^+\pi^-\gamma$ hypothesis, it was possible that the remaining sample contained some $K^-p \rightarrow \Lambda\pi^+\pi^-$ events. Also it was quite possible for a $K^-p \rightarrow \Lambda\eta$ event to fit the $K^-p \rightarrow \Lambda\pi^+\pi^-\gamma$ hypothesis. To remove these unwanted events from the sample, the effective mass of the (Λ,γ) was required to be within 0.012 GeV of 1.192 GeV, the accepted mass of the Σ°. Having completed the above cuts,

1,509 events were determined to have proceeded by the $K^- p \rightarrow \Sigma^\circ \pi^+ \pi^-$ reaction. These events were examined for the Y_1^* resonance.

The histogram representing the mass squared distribution if every π^+ had resonated with the Σ°'s is presented in Figure 15. The corresponding histogram for the (Σ°, π^-) combination is given in Figure 16. Inspection of Figures 15 and 16 yield no strong evidence of any Breit-Wigner shaped humps which could indicate Y_1^* production. But neither do the distributions correspond to only non-resonant three body interactions. This is apparent by looking at the normalized phase space functions drawn in Figures 15 and 16. The chi squares for a pure phase space fit to the $M^2(\Sigma^\circ, \pi^+)$ and $M^2(\Sigma^\circ, \pi^-)$ histograms are 170 and 160 with 24 degrees of freedom respectively. Any attempt to fit a linear combination of Breit-Wigner and phase space distribution functions to the mass squared distributions given in Figures 15 and 16 proved unsuccessful. Coherent interference of Breit-Wigner and phase space was also tried unsuccessfully. Furthermore, an examination of the Dalitz Plot (Figure 17) shows little evidence that the Y_1^{*+} and Y_1^{*-} overlap on the plot. Hence no attempt was made to determine if there was interference between the two charged states.

Since all attempts had failed to fit the histograms, we again proceeded to determine which π might have resonated with each Σ°. The same procedure was followed as with the $K^- p \rightarrow \Lambda \pi^+ \pi^-$ events described in section A. Just as with the Λ's, no geometric or kinematic basis could be found for the selection of the proper π. Again, upon applying our procedure of allocating part of each event to a positive and negative histogram, there was a very noticeable improvement in the chi squares. The results of the best fits appear in Table II. The corresponding experimental histograms and theoretical functions are shown in Figures 18 and 19.

Figure 15: Pure phase space fit to $M^2(\Sigma^\circ, \pi^+)$ histogram. Each Σ° combined with π^+.

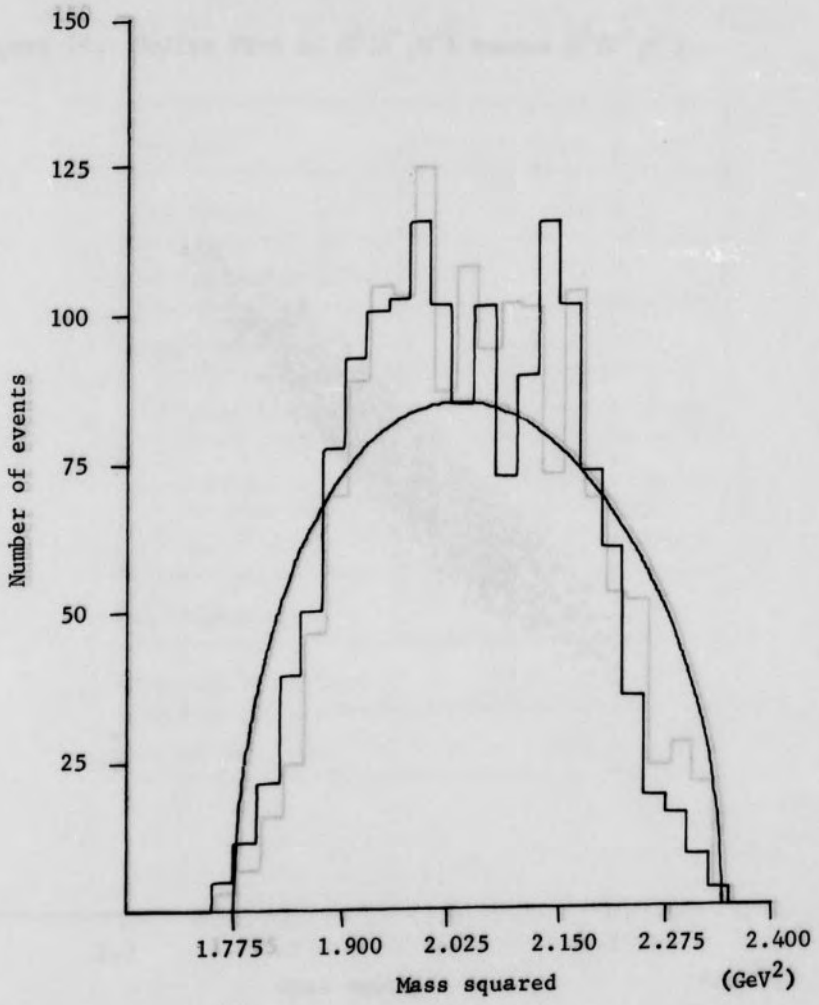

Figure 16: Pure phase space fit to $M^2(\Sigma^\circ,\pi^-)$ histogram. Each Σ° combined with π^-.

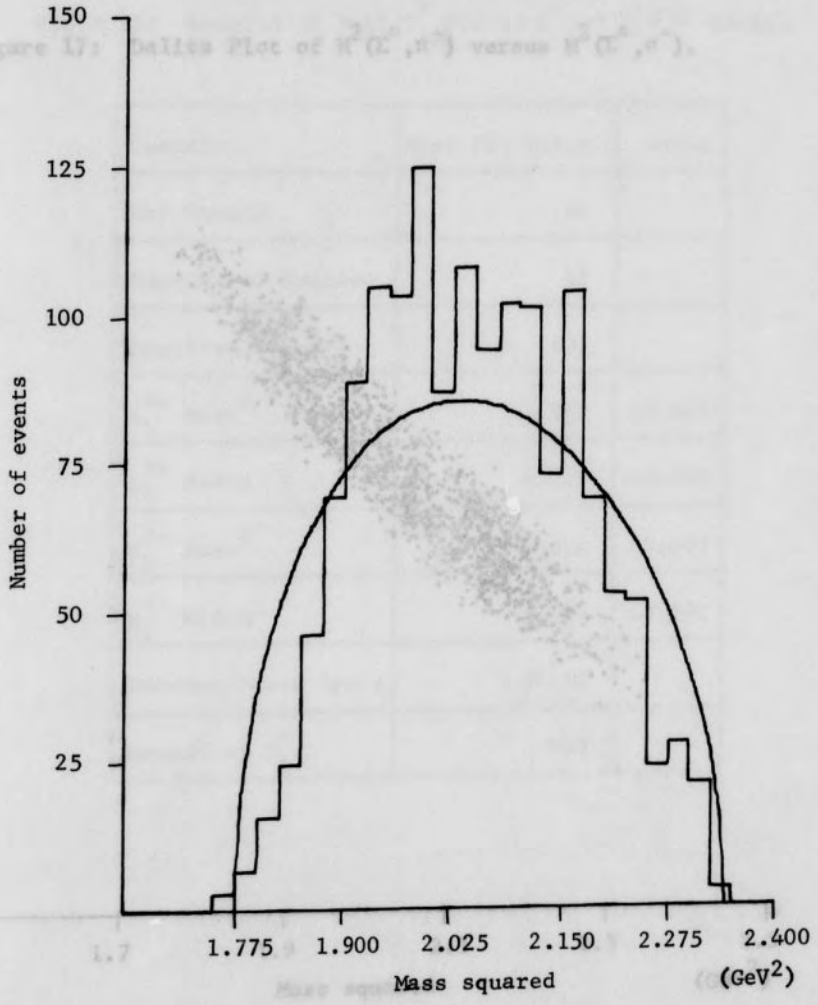

Figure 17: Dalitz Plot of $M^2(\Sigma^\circ,\pi^+)$ versus $M^2(\Sigma^\circ,\pi^-)$.

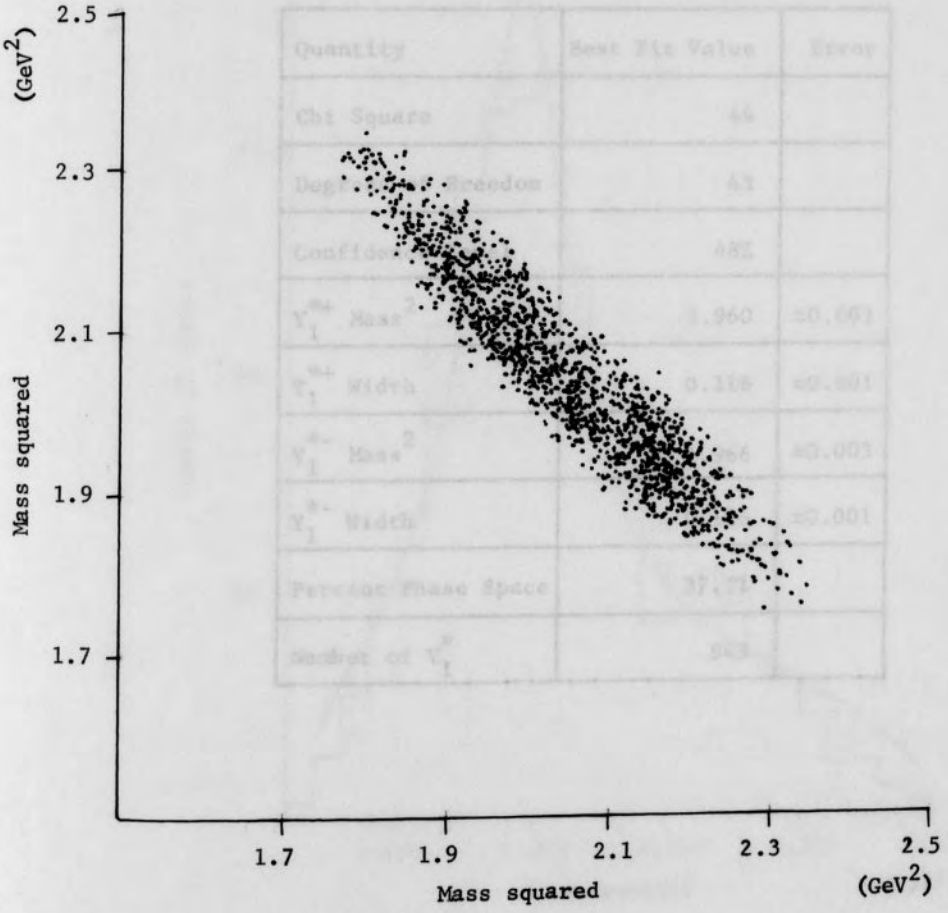

Table II: Results of Best Y_1^* Fit to $K^-p \rightarrow \Sigma^\circ\pi^+\pi^-$ Events

Quantity	Best Fit Value	Error
Chi Square	44	
Degrees of Freedom	43	
Confidence Level	48%	
Y_1^{*+} Mass^2	1.960	±0.003
Y_1^{*+} Width	0.116	±0.001
Y_1^{*-} Mass^2	1.966	±0.003
Y_1^{*-} Width	0.116	±0.001
Percent Phase Space	37.5%	
Number of Y_1^*	943	

Figure 18: Allocation fit to $M^2(\Sigma^\circ,\pi^+)$ histogram.

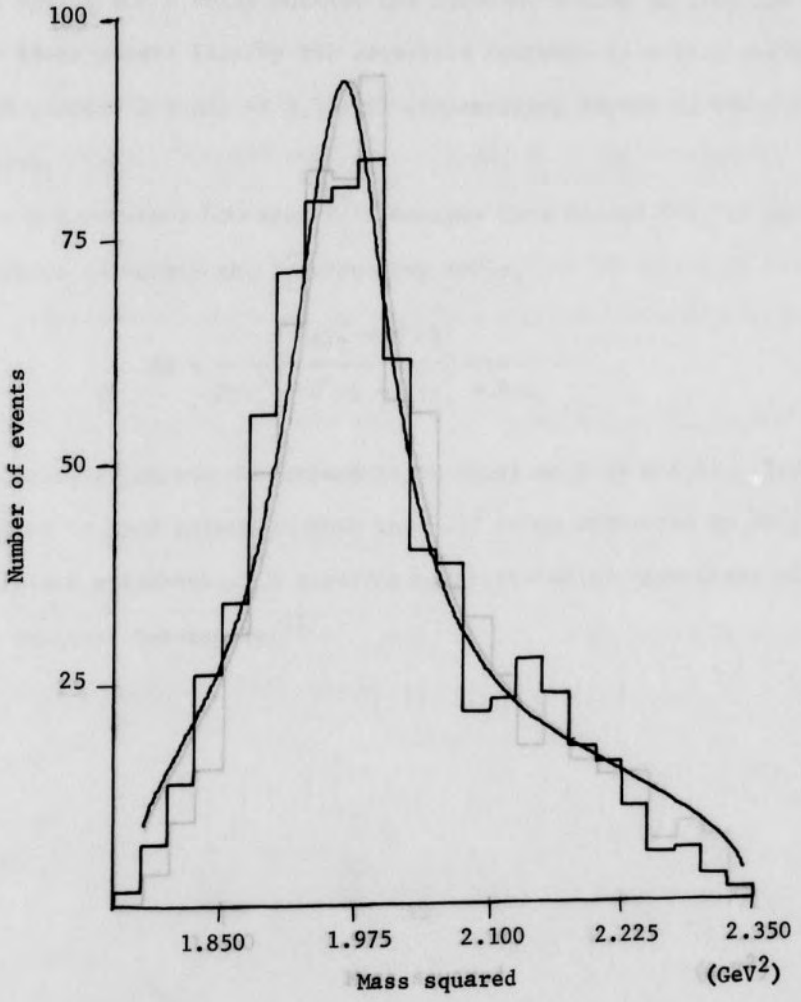

Figure 19: Allocation fit to $M^2(\Sigma^\circ,\pi^-)$ histogram.

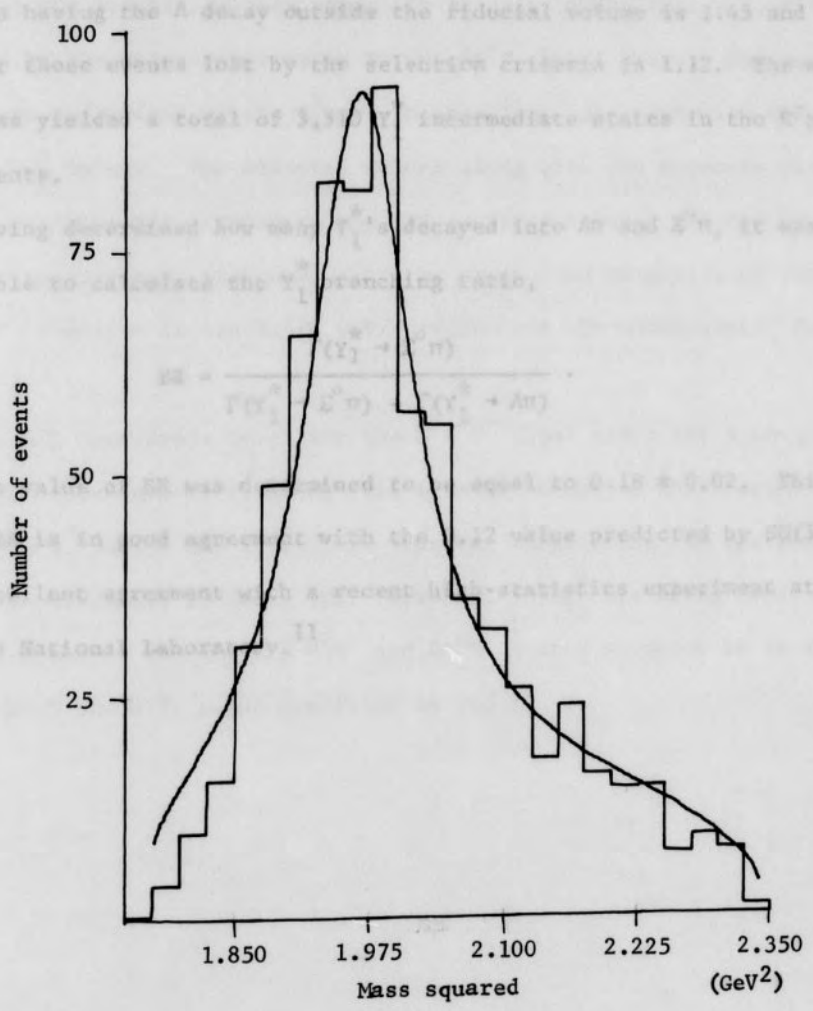

To determine the number of Y_1^* states in the $K^-p \rightarrow \Sigma^\circ\pi^+\pi^-$ events of all the data, each Y_1^* state found in the sample of events was weighted by a factor of 3.51. The weighting factor is the product of the same weights as used for the Λ's with the following two exceptions. The weight for the events having the Λ decay outside the fiducial volume is 1.45 and the weight for those events lost by the selection criteria is 1.12. The weighting process yielded a total of 3,310 Y_1^* intermediate states in the $K^-p \rightarrow \Sigma^\circ\pi^+\pi^-$ events.

Having determined how many Y_1^*'s decayed into $\Lambda\pi$ and $\Sigma^\circ\pi$, it was now possible to calculate the Y_1^* branching ratio,

$$BR = \frac{\Gamma(Y_1^* \rightarrow \Sigma^\circ\pi)}{\Gamma(Y_1^* \rightarrow \Sigma^\circ\pi) + \Gamma(Y_1^* \rightarrow \Lambda\pi)} .$$

The value of BR was determined to be equal to 0.18 ± 0.02. This value of BR is in good agreement with the 0.12 value predicted by SU(3),[10] and in excellent agreement with a recent high-statistics experiment at Brookhaven National Laboratory.[11]

CHAPTER V

SUMMARY AND CONCLUSIONS

From the results of this study, it is quite clear that $Y_1^*(1385)$ production is the major contributor to the $\Lambda\pi^+\pi^-$ final state. The measured masses and widths of the Y_1^* are in excellent agreement with the world average values. The measured values along with the accepted values are shown in Table III. However, the 16% confidence level for the fit which gave those values indicates that the production mechanism of the $K^-p \rightarrow \Lambda\pi^+\pi^-$ reaction in the 1.670 GeV/c region was not conclusively determined.

The 48% confidence level for the $\Sigma^\circ\pi^+\pi^-$ final state fit strongly indicates the presence of $Y_1^*(1385)$ with a large amount of phase space background. The Y_1^* masses and widths are somewhat larger than the accepted values which are shown in Table III. However, the Y_1^* branching ratio of the $\Sigma^\circ\pi^+\pi^-$ state to the total $\Sigma^\circ\pi^+\pi^-$ and $\Lambda\pi^+\pi^-$ states produced is in good agreement with the 0.12 value predicted by SU(3).

Table III: Comparison of Experimental and Accepted Values

Quantity	World Average Value[12]	Experimental Values $Y_1^* \rightarrow \Lambda\pi$	$Y_1^* \rightarrow \Sigma^\circ\pi$
Y_1^{*+} Mass	1382.8 ±0.7	1385 ±4	1400 ±1
Y_1^{*+} Width	35.9 ±2.6	36.2 ±0.7	41.4 ±0.3
Y_1^{*-} Mass	1385.9 ±1.5	1382 ±3	1403 ±1
Y_1^{*-} Width	36.3 ±6.3	35.4 ±0.7	41.4 ±0.3

Note: For explanation of experimental errors see page 27. Units are MeV

FOOTNOTES AND BIBLIOGRAPHY

1. P. Nyborg and O. Skjaggestad, "Notes on Phase Space," University of Oslo, Norway (February, 1967).

2. B. T. Feld, Models of Elementary Particles (Blaisdell Publishing Co., Waltham, Massachusetts, 1969), p. 147.

3. E. Segre, Nuclei and Particles (W. A. Benjamin, Inc., New York, 1965), p. 313.

4. W. R. Frazer, Elementary Particles (Prentice Hall, Inc., Englewood Cliffs, New Jersey, 1966), Chapter 5, pp. 69-83.

5. T. Snow, "Three Body Cross Sections in K^-p Interactions at 1670 MeV," Ph. D. Dissertation, Duke University (1971), pp. 43-49.

6. Reference 5, pp. 72.

7. G. W. Meisner, private communication.

8. R. B. Muir, private communication.

9. Reference 5, pp. 44, 56.

10. N. P. Samios, M. Goldberg and B. Meadows, "Hadrons and SU(3): A Critical Review," Brookhaven National Laboratory publication number BLN 17851, (May, 1973), p. 20.

11. S. R. Borenstein, G. R. Kalbfleisch, R. C. Strand, V. Vanderburg and J. W. Chapman, "A Determination of the Mass, Width and the $(\Sigma\pi/\Lambda\pi)$ Branching Ratio of the $\Sigma(1385)$ Baryon," Brookhaven National Laboratory publication number BNL 18665, (February, 1974), p. 1.

12. "Review of Particle Properties," supplement to Reviews of Modern Physics (American Institute of Physics, Lancaster, Pa., April, 1973) Volume 45, pp. 152-154.

APPENDIX A

The kinematics at a production or decay vertex can be completely described by four equations. Three of these are conservation of momentum. The fourth is the conservation of energy equation. With four equations, it is possible to determine four unknowns. Thus, for an event containing both production and decay vertices, there are eight equations which can be used to calculate eight variables. In other words, the number of degrees of freedom for such an event type must be eight or less. If the energies and momenta of all the particles can be determined from measured quantities, then the reaction hypothesis is said to have eight degrees of freedom. However, if one or more of the energies and momenta can not be determined from measured quantities, then each missing variable must be calculated using one of the eight equations. This reduces the number of equations available to calculate unknowns; in other words, the number of degrees of freedom is reduced. For example, in the $K^-p \rightarrow \Lambda\pi^+\pi^-$ hypothesis, the magnitude of the Λ's momentum must be calculated from one of the equations because only the direction of the momentum can be measured (a neutral particle does not leave a track in a bubble chamber). Thus, the $K^-p \rightarrow \Lambda\pi^+\pi^-$ hypothesis has only seven degrees of freedom.